Hydrogen dissociation on metal surfaces

Wijzenbroek, M.

CHAPTER 7

Ab initio molecular dynamics study of D_2 dissociation on CO-precovered Ru(0001)

This chapter is based on:

M. Wijzenbroek and G. J. Kroes. *Ab initio* molecular dynamics study of D_2 dissociation on CO-precovered Ru(0001). *Physical Chemistry Chemical Physics*, accepted for publication. 2016.

Abstract

In dynamics calculations of H_2 dissociating on metal surfaces often clean, high-symmetry surfaces are used. Few such dynamics studies have been performed on surfaces with pre-adsorbed molecules, and even fewer studies also consider the motion of the surface and the adsorbate. In this study, the dissociation of H_2 on a carbon monoxide-covered Ru(0001) surface is considered. *Ab initio* molecular dynamics (AIMD) calculations are performed on this system using the PBE-vdW-DF2 functional, which accurately describes the reaction probability for H_2 dissociation on Ru(0001). Using this functional, the reaction probability of H_2 on the CO-covered Ru(0001) surface is found to be too low compared to experiments. This suggests that exchange–correlation functionals that can describe reaction of H_2 on a bare metal surface are not in general able to describe the reaction of H_2 on a CO-precovered surface of the same metal, with the same accuracy. It can however not be ruled out that the discrepancy between theory and experiment is partly due to an inhomogeneous coverage of the surface by CO in the experiments. The incorporation of the motion of the surface has only a small effect on the reaction probability. It is found that when including surface motion for this system, the size of the simulation cell can be important. Upon collision, a considerable amount of energy is transferred to the surface, causing the adsorbed CO molecules to move apart, which opens the surface for reaction. In order to obtain converged reaction probabilities with respect to the size of the simulation cell, at least a 3×3 simulation cell is needed, because in the smaller $\sqrt{3} \times \sqrt{3}$ cell the CO molecules cannot be pushed apart as only a single independent CO molecule is present, also leading to less energy exchange with the surface.

7.1 Introduction

In detailed dynamics simulations of hydrogen molecules reacting on metal surfaces often clean, high-symmetry surfaces are used.[1] Only few dynamics studies have been performed on surfaces which have been pre-covered with, for example, H atoms or CO molecules, and even

fewer studies have allowed the surface atoms and the pre-adsorbed atoms or molecules to move. Such studies have been performed for H_2 dissociation on various palladium surfaces decorated with H, S or Cl atoms.[2–7] No studies with a non-rigid surface have however been performed yet for the dissociation of H_2 or D_2 on a CO-covered surface, which are of interest because CO acts as a common poison for catalysts.

An example of such a system, for which sticking probabilities have been experimentally measured, is D_2 dissociation on a CO-covered Ru(0001) surface.[8] This system has already been studied with extensive density functional theory (DFT) calculations[9] and with dynamics calculations,[10] but in the dynamics calculations the CO and the surface atoms were fixed at their ideal lattice positions. Although no large surface temperature effects would be expected at the rather low experimental surface temperature ($T_s = 180\,K$[8]), it has not yet been tested whether or not allowing the surface atoms and CO molecules to move may improve the description of the process. In particular, a relevant question is whether or not the D_2 can exchange energy with the CO molecules. The masses of the D_2 and CO molecules match better than those of D_2 and Ru, suggesting energy exchange may play a large role in the dynamics, as the simple Baule model suggests that energy exchange becomes important if the masses of the projectile and the surface atoms match.[11,12] Finally, Zhao *et al.*[13] have studied co-adsorption of H_2 and CO on Ru(0001) with DFT, considering precoverages of Ru(0001) by CO other than the 1/3 monolayer (ML) precoverage considered here. With the RPBE functional used, they obtained reasonable agreement with ultrahigh vacuum experiments for their computed CO and H_2 desorption temperatures and patterns.

The underlying surface system (CO on Ru(0001)) has been the subject of many different studies in which, *e.g.*, CO adsorption and desorption, surface structures and vibrations have been studied, both from an experimental[14–39] and a theoretical[13,38–52] point of view. At different CO coverages, different surface structures are observed. For low coverages of up to 1/3 ML, CO molecules tend to adsorb on top sites.[15,16,43–45] For CO on Ru(0001), the CO molecules adsorb with an orientation perpendicular to the surface, with the C atom bonded to the surface.[14–18] One particularly well-studied system is 1/3 ML CO on Ru(0001) (for a com-

parison of experimental and theoretical data, see reference 9), which exhibits a $(\sqrt{3}\times\sqrt{3})$R30° geometry, which seems to be the best defined CO-covered Ru(0001) surface,[9,45] with the CO molecules occupying one in every three top sites. For this reason, and because previous theoretical studies[9,10] of D_2 dissociation on CO-covered Ru(0001) have also considered this particular coverage, the 1/3 ML case is considered in this study.

For H_2 and D_2 dissociation on a bare Ru(0001) surface, two DFT exchange–correlation (XC) functionals were found in chapter 4 that could describe the reaction probability well over the range of incidence energies for which experiments[53] are available. Previous calculations[54] showed that the reaction could not be well described by the PW91[55] (or the similar PBE[56]) and RPBE[57] XC functionals, which are commonly used for studies of molecules dissociating on metal surfaces. A mixture of these functionals allowed several experiments on H_2 dissociation on Cu(111) to be reproduced with chemical accuracy.[58] For H_2 dissociation on Ru(0001) however, these functionals yielded reaction probabilities that increased too quickly with increasing incidence energy. It was, for this system, found that using functionals with either vdW-DF[59] or vdW-DF2[60] correlation results in an improved agreement of the reaction probability with experiments.

The description of CO-covered surfaces with DFT has received a lot of attention. For example, the popular PW91, PBE and RPBE functionals fail to predict the correct adsorption site of the CO molecule on the Pt(111) surface.[61] Also for other surfaces (Cu(111) and Rh(111)) the wrong adsorption site preference is found,[42] giving rise to the "CO adsorption puzzle".[46] Using higher level electronic structure calculations, *e.g.*, hybrid functionals (B3LYP[46] and PBE0 and HSE03[62]), the random phase approximation (RPA),[63] the revTPSS meta-generalized gradient approximation (meta-GGA) functional[49] or vdW-DF functionals[64] partially or fully resolves this problem. For 1/3 ML CO-covered Ru(0001) the correct adsorption site (top) is already predicted at the generalized gradient approximation (GGA) level.[9]

In this chapter, *ab initio* molecular dynamics (AIMD) calculations are performed to describe D_2 dissociation on a 1/3 ML CO-covered Ru(0001) surface, to understand if allowing the CO molecules and the

surface atoms to move has effects on the dynamics. A second aspect, however, is the use of the XC functional. Dynamics calculations have previously been performed for H_2 dissociation on CO-covered Ru(0001) with the RPBE[57] functional.[10] This functional however yielded reaction probabilities that were too low compared to experiments that have been performed for this system.[8] Recently, two functionals have been identified using a specific reaction parameter (SRP)[58] approach that can accurately describe the dissociation of H_2 on a bare Ru(0001) surface, which is not possible with the RPBE functional (see also chapter 4). These functionals use either vdW-DF[59] or vdW-DF2[60] correlation. An interesting question is whether these functionals can also properly describe H_2 dissociation on a CO-covered Ru(0001) surface.[65] For the present study one of the two candidate SRP functionals for H_2 dissociation on Ru(0001), the PBE-vdW-DF2 functional, is taken.

In section 7.2 the methods used are described, starting with the dynamical model in section 7.2.1. Initial and analysis conditions are described in section 7.2.2 and the computational details in section 7.2.3. In section 7.3 the results are presented and discussed, starting with properties of the surface in section 7.3.1. The molecule–surface interaction is explored in section 7.3.2. The reaction probability, its comparison to experiments as well as differences between the results obtained with different unit cell sizes are discussed in section 7.3.3. Finally, in section 7.4 the conclusions are given.

7.2 Methods

7.2.1 Dynamical model

In all calculations the Born–Oppenheimer[66] approximation is used. Two types of calculations are performed: calculations in which the surface atoms are allowed to move at the experimental surface temperature ($T_s = 180\,\mathrm{K}$), and calculations in which the surface atoms are frozen at their ideal lattice positions. The forces and energies needed for the dynamics were determined "on the fly" from DFT[67,68] calculations. For the DFT calculations the PBE-vdW-DF2[56,60] functional was used, which was in chapter 4 found to be able to describe the dissociation of H_2 and

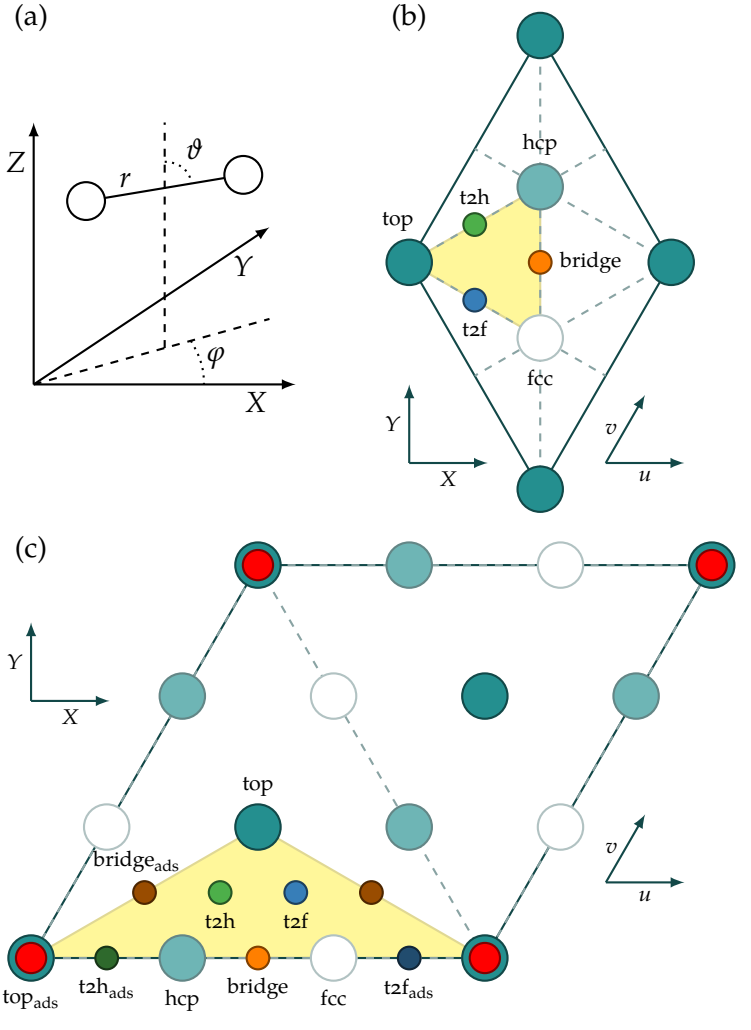

FIGURE 7.1 (a) The center of mass coordinate system used to describe the coordinates of the H_2 molecule. (b) The surface unit cell considered for the H_2/Ru(0001) system. (c) The $\sqrt{3} \times \sqrt{3}$ surface unit cell considered for the H_2/CO+Ru(0001) system. The diagonal of the $\sqrt{3} \times \sqrt{3}$ unit cell coincides with one of the lattice vectors of the 3×3 cell. In (b) and (c), several sites which are commonly considered are indicated. The subscript "ads" in (c) is used to indicate which site is nearest the adsorbed CO, for sites that are, due to addition of CO, no longer symmetry equivalent.

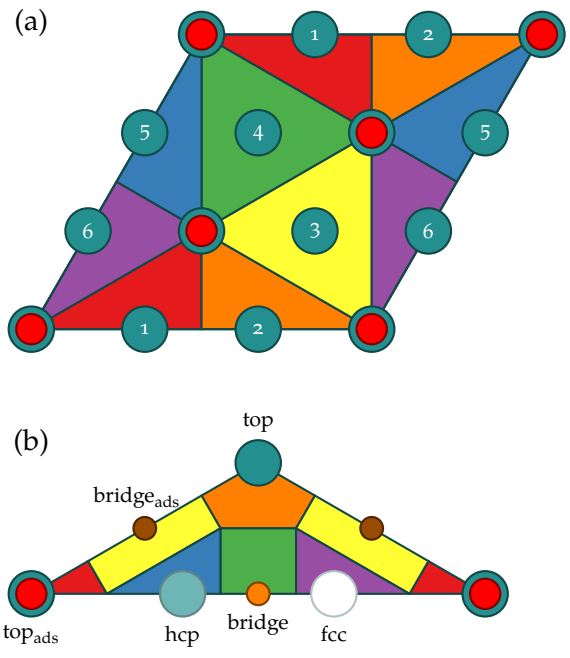

Figure 7.2 (a) The six triangles spanned by the CO molecules for the 3×3 cell. Each triangle has three CO molecules that can move independently. (b) The bins used to compute site-specific properties. The sites giving names to the bins have been indicated (see also figure 7.1(c)).

D_2 on Ru(0001) rather accurately.

In the dynamics calculations for $T_s = 180\,\mathrm{K}$, the motion of all atoms of the D_2 molecule and the CO-covered Ru(0001) slab is taken into account, except for the bottom layer of the Ru(0001) slab, which remains fixed during the dynamics. For the ideal lattice calculations, the whole slab, including the layer of CO molecules, remains fixed during the dynamics and only the D_2 molecule is allowed to move. Calculations were done both using a $\sqrt{3} \times \sqrt{3}$ and a 3×3 cell, but for the ideal lattice calculations only a $\sqrt{3} \times \sqrt{3}$ cell was used. In figure 7.1 the coordinate system that is used to describe the location of the H_2 molecule, the surface unit cell for bare Ru(0001), and the $\sqrt{3} \times \sqrt{3}$ surface unit cell of 1/3 ML CO-covered Ru(0001) are shown. It is noted that if the surface atoms are allowed to move, the molecule–surface distance Z is generally ill defined. Throughout this chapter the convention is used that the highest atom

that is part of the slab (including the adsorbate; for the CO-covered surface this is therefore generally an oxygen atom of a CO molecule on the surface) determines the location for $Z = 0$ Å. Negative Z values thus correspond to the H_2 molecule being in the CO layer of the slab.

In figure 7.2 two schemes used for analysis are shown. In figure 7.2(a), the six triangles that are spanned by the CO molecules in a 3×3 cell are shown. These triangles are used to analyse the amount of freedom a molecule has to dissociate on different parts of a slab at a finite surface temperature. Each triangle has three CO molecules at the corners of the triangle that are, to a large extent, free to move relative to the surface. This is in contrast to the $\sqrt{3} \times \sqrt{3}$ cell, in which only one single independent CO is present. In figure 7.2(b), the bins used to obtain site-specific properties are shown. The names of the bins are derived from the site that is located at the center of the bins in the ideal, static surface.

In the dynamics, the equations of motion are integrated using the leapfrog propagator with a time step of 1 fs for the slab equilibrations, and a time step of 0.5 fs, 0.25 fs or 0.125 fs for ($v = 0$), ($v = 1$) and ($v \geq 2$) D_2, respectively.

7.2.2 Initial and analysis conditions

Quasi-classical dynamics calculations are performed, in which zero-point energy (ZPE) is imparted to the D_2 initially. The initial rovibrational energy that is put into the D_2 molecule is determined by the Fourier grid Hamiltonian method.[69] An ensemble of D_2 molecules in various rovibrational states and with various translational energies corresponding to the experimental distribution in the molecular beam is considered. This procedure, including the parameters used for these distributions, is the same as used for the H_2 dissociation on Ru(0001) calculations of chapter 4.

The H_2 molecule is initially placed at $Z = 6.5$ Å. The molecule is considered to have scattered if $Z > 4.0$ Å with a momentum vector away from the surface. The molecule is considered to have dissociated if $r > 2.0$ Å. Molecules that have neither reacted nor dissociated after 1 ps (2 ps for the highest energy point), are considered to have scattered.

To generate the initial conditions of the slab and CO molecules, several steps are performed. First, the bulk lattice constants a and c for Ru are determined by relaxing a HCP unit cell with two atoms. No thermal expansion is taken into account, as Ru at $T_s = 180$ K is very similar to Ru at $T_s = 0$ K (from 0 K to 180 K, the a and c lattice constants grow by 0.05% and 0.08%, respectively).[70] The ideal slab geometry is then determined by allowing all atoms of a CO-covered slab, except the bottom layer, to relax in the z direction. Vibrational frequencies are then determined for each of the atoms that are allowed to move in the slab, while keeping the other atoms fixed. These vibrational frequencies are then used to initialize random displacements for the atoms of the slab. Initial velocities for the surface atoms are taken from a Maxwell–Boltzmann distribution. For the $\sqrt{3} \times \sqrt{3}$ cell, 50 randomly determined configurations are taken. Each of these 50 snapshots is propagated for in total 4.0 ps with a time step of 1.0 fs. During the first 1.0 ps velocities are rescaled every 5 (first 0.5 ps) and 50 (second 0.5 ps) time steps. After the velocity rescaling, the calculation proceeds in the NVE ensemble, of which the first 0.5 ps is discarded. Initial conditions for the slab and CO molecules are then randomly selected from the remaining 2.5 ps, giving in total 125×10^3 possible sets of initial conditions spread over the different slabs. For the 3×3 cell, the same procedure is used, except that only 20 slabs are propagated due to the increased size of the simulation cell.

7.2.3 Computational details

The electronic structure calculations were done with version 5.2.12 of the VASP[71–74] software package. The standard[74] projector augmented wave (PAW)[75] potentials were used. The non-local vdW-DF2 correlation functional in VASP is evaluated within the scheme of Román-Pérez and Soler.[76]

To speed up convergence, first order Methfessel–Paxton[77] smearing was used with a smearing width of 0.1 eV. For the bulk calculation, a $20 \times 20 \times 20$ Γ-centered k-point grid was used with a plane wave cutoff of 500 eV. For all other calculations, a $9 \times 9 \times 1$ Γ-centered (shifted Monkhorst–Pack[78]) k-point mesh was used for calculations with the $\sqrt{3} \times \sqrt{3}$ unit cell, while a $5 \times 5 \times 1$ Γ-centered k-point mesh was used for

the 3 × 3 cell. A plane wave cutoff of 400 eV was used. For both cells a vacuum of 13 Å was chosen to separate different images of the slab. In all cases a five layered ruthenium slab was considered, with either one or three CO molecules adsorbed on one side, for the $\sqrt{3} \times \sqrt{3}$ and 3 × 3 cells, respectively. Convergence tests for the potential energy suggest that the error introduced due to the basis set size, k-point integration and the number of Ru layers is less than 30 meV. Tests with CO molecules adsorbed on both sides of the slab suggest barrier heights may be decreased by at most about 20 meV.

To obtain accurate statistics, 500 trajectories are computed for two energy points of interest on the reaction probability curve. Only for the highest energy point with the $\sqrt{3}\times\sqrt{3}$ cell for $T_s = 180$ K, 1000 trajectories are computed. Throughout this chapter, observables are often denoted by $O \pm \sigma$, where σ is an approximation of the statistical errors due to the limited number of trajectories, and is approximated by $\sigma = s/\sqrt{nN}$, where s is the sample standard deviation, N the number of trajectories and n the number of samples per trajectory. For reaction probabilities, $\sigma = \sqrt{P_r \cdot (1 - P_r)}/\sqrt{N}$, where P_r is the computed reaction probability.

7.3 Results and discussion

7.3.1 Properties and dynamics of the CO-covered surface

The adsorption energies (defined as $E_{ads} = E_{CO} + E_{Ru} - E_{CO/Ru}$) for CO above a five layer Ru slab on the top and hcp sites are found to be 1.91 eV and 1.65 eV, respectively. These numbers match quite well to the adsorption energies computed by Groot *et al.*[9] and the top site adsorption energy is in good agreement with the measured adsorption energy of Pfnür and Menzel[23] for 1/3 ML (1.81 eV), but less so with the adsorption energy from an earlier study (1.66 eV) by the same authors[24] and the experimental value reported by Abild-Pedersen and Andersson[48] (1.49 ± 0.22 eV). It is noted that it is not clear how this value was determined (multiple experiments were cited) and at which coverage, which should be important: Pfnür and Menzel[23] found the adsorption energy to depend on the CO coverage of the surface.

In table 7.1 several geometrical parameters of the 1/3 ML CO-

Table 7.1 Several geometrical parameters obtained with dynamics calculations on the CO-covered Ru(0001) surface. The meaning of the symbols is explained in the text. The values for D_2 dissociation correspond to averages over the (whole) computed trajectories for $E_{trans} = 0.466\,eV$.

Property	Relaxed	$\sqrt{3}\times\sqrt{3}$	(+ D_2)	3×3	(+ D_2)	Experiment
$\langle\sigma_O\rangle$ (Å)	0	0.337	0.425	0.341	0.567	—
$\langle\sigma_C\rangle$ (Å)	0	0.216	0.270	0.214	0.347	—
$\langle\sigma_{CO}\rangle$ (Å)	0	0.278	0.351	0.280	0.468	—
$\langle\sigma_O^{\parallel}\rangle$ (Å)	0	0.330	0.414	0.335	0.559	0.5 ± 0.1[16]
$\langle\sigma_C^{\parallel}\rangle$ (Å)	0	0.207	0.257	0.206	0.339	0.3 ± 0.1[16]
$\langle\sigma_O^{\perp}\rangle$ (Å)	0	0.061	0.093	0.058	0.096	0.1[16]
$\langle\sigma_C^{\perp}\rangle$ (Å)	0	0.056	0.077	0.055	0.071	0.1[16]
$\langle\vartheta_{C-O}\rangle$ (°)	0	7.7	9.4	7.9	11.1	—
$\langle\vartheta_{Ru-O}\rangle$ (°)	0	5.6	7.0	5.7	9.2	—
$\langle d_{1-2}\rangle$ (Å)	2.137	2.139	2.134	2.139	2.137	2.094[79]
$\langle d_{prot}\rangle$ (Å)	0.184	0.165	0.147	0.169	0.164	0.07 ± 0.03[27]
$\langle r_{Ru-C}\rangle$ (Å)	1.915	1.920	1.918	1.920	1.923	1.93 ± 0.04[27]
$\langle r_{C-O}\rangle$ (Å)	1.165	1.166	1.167	1.166	1.167	1.10 ± 0.05[27]

covered Ru(0001) surface are shown, comparing the small and large simulation cells with and without the D_2 molecule impinging on the surface. All properties are ensemble averages, which in the context of the present calculations means that averages are taken over, if applicable, one or more occurrences in the unit cell and the different trajectories that were performed. Several types of properties are considered: average root mean square displacements (σ_x) of atoms ($x = C, O$) or the CO center of mass ($x = CO$) with respect to its position in the case of the ideal lattice, the parallel ($\sigma_x^{\parallel}$) or perpendicular ($\sigma_x^{\perp}$) components of the average root mean square displacements, the angle of a vector from atom a to b with respect to the surface normal (ϑ_{a-b}), the first interlayer spacing (d_{1-2}, average distance between the two topmost Ru layers of the surface), the protrusion of the Ru atom directly below the CO molecule with respect to the other Ru atoms in that layer (d_{prot}), and bond lengths (r_{a-b}) between atoms a and b. Many of these parameters

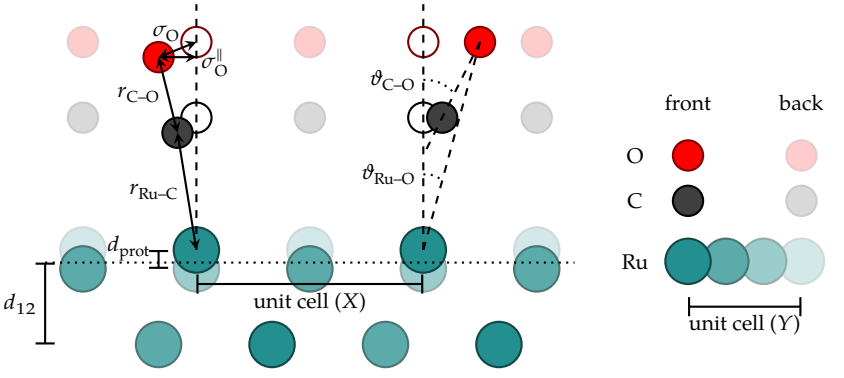

Figure 7.3 Schematic side view (left) of the 1/3 ML CO-covered Ru(0001) surface. The shown view is along the Y-axis for the $\sqrt{3} \times \sqrt{3}$ cell of figure 7.1(c), starting at the bottom (the U or X-axis). The frontmost two CO molecules have been displaced from their ideal positions (open circles). The geometrical parameters of table 7.1 are indicated and are explained in more detail in the text. Atoms that are further away are indicated by faded circles (see right figure).

are also shown in figure 7.3. In table 7.1, with a subscript Ru the Ru atom immediately below a C or O atom of a CO molecule is meant. The results for the cases with the D_2 molecule impinging on the surface are discussed in section 7.3.3; for the case without the D_2 molecule the results are discussed below.

The distance between the topmost ruthenium atom and the C atom, as well as the distance between the C and O atoms, has been measured by Michalk *et al.*[15] and Over *et al.*[27] The values found here for all cases (1.92 Å for the r_{Ru-C} distance and 1.17 Å for r_{C-O}) match quite well to the experimental values by Over *et al.* (1.93 ± 0.04 Å and 1.10 ± 0.05 Å, respectively) and Michalk *et al.* (2.00 ± 0.10 Å and 1.10 ± 0.10 Å, respectively), although the computed C–O distance is a bit on the long side. The root mean square displacement of the C and O atoms has been measured by Gierer *et al.*[16] and Over *et al.*[27,28] The computed displacements are in fair agreement with the results of the latest experiment[16] (0.5 ± 0.1 Å for $\sigma_O^{\parallel}$ at $T_s = 150$ K and 0.3 ± 0.1 Å for $\sigma_C^{\parallel}$). The protrusion of the Ru atom to which the CO is attached with respect to the other atoms in the layer is somewhat larger than the experimental value (0.07 ± 0.03 Å) by Over *et al.*[27] The contraction of the distance between

the first and second layer is about 1.5% compared to the computed bulk interlayer spacing (2.169 Å), which is a bit smaller than the value for the bare Ru(0001) surface with the DFT functional used (3.3%). At T_s = 300 K, Baddorf *et al.*[79] measured the contraction of the distance between the first and second layer to be 2.2 ± 0.4%, corresponding to a first interlayer spacing of about 2.094 Å. Finally, the results are overall in good agreement with DFT studies[9,45] in which the RPBE functional was used.

Another interesting property concerns the motion of CO with respect to the surface. From the C and O displacements given above, it is clear that although the molecule has some freedom to move, it does not readily move to the next top site (about 2.7 Å away). The fact that the displacement of the CO center of mass (σ_{CO}) closely matches the weighted average of the displacements of the individual C and O displacements, as well as that the Ru–C and C–O distances remain similar during the dynamics as in the static surface case, suggests that the molecules behave in a way similar to that proposed by Gierer *et al.*[16]: the CO molecule tilts with respect to the topmost Ru atom, keeping the topmost Ru to which the CO is adsorbed, and the C and O atoms approximately on a line. Tilt angles of the line connecting the two atoms with respect to the surface normal (ϑ_{C-O} and ϑ_{Ru-O}) have been computed. ϑ_{Ru-O} is slightly smaller (by about 2°) than ϑ_{C-O}, suggesting that the C atom is on average not displaced far enough for the Ru, C and O atoms to be on a line. Although the tilt angles are not large, the tilting of the CO molecules may nonetheless have an effect on the H_2 dissociation dynamics. A small decrease in reactivity might be expected, because more of the surface is "screened" by the CO for the impinging D_2 molecules.

7.3.2 The molecule–surface interaction

In figure 7.4 contour plots of the PES for H_2 dissociation on an ideal 1/3 ML CO-covered Ru(0001) surface ($\sqrt{3} \times \sqrt{3}$ cell) are shown for dissociation above various sites and orientations with $\vartheta = 90°$. It is clear that near a CO-covered Ru atom it is rather unfavourable for the H_2 molecule to dissociate, although for dissociation above hcp or bridge$_{ads}$ nonetheless a barrier and an exit channel is found. In contrast, for the cases where the H_2 molecule is near a Ru atom without an adsorbed

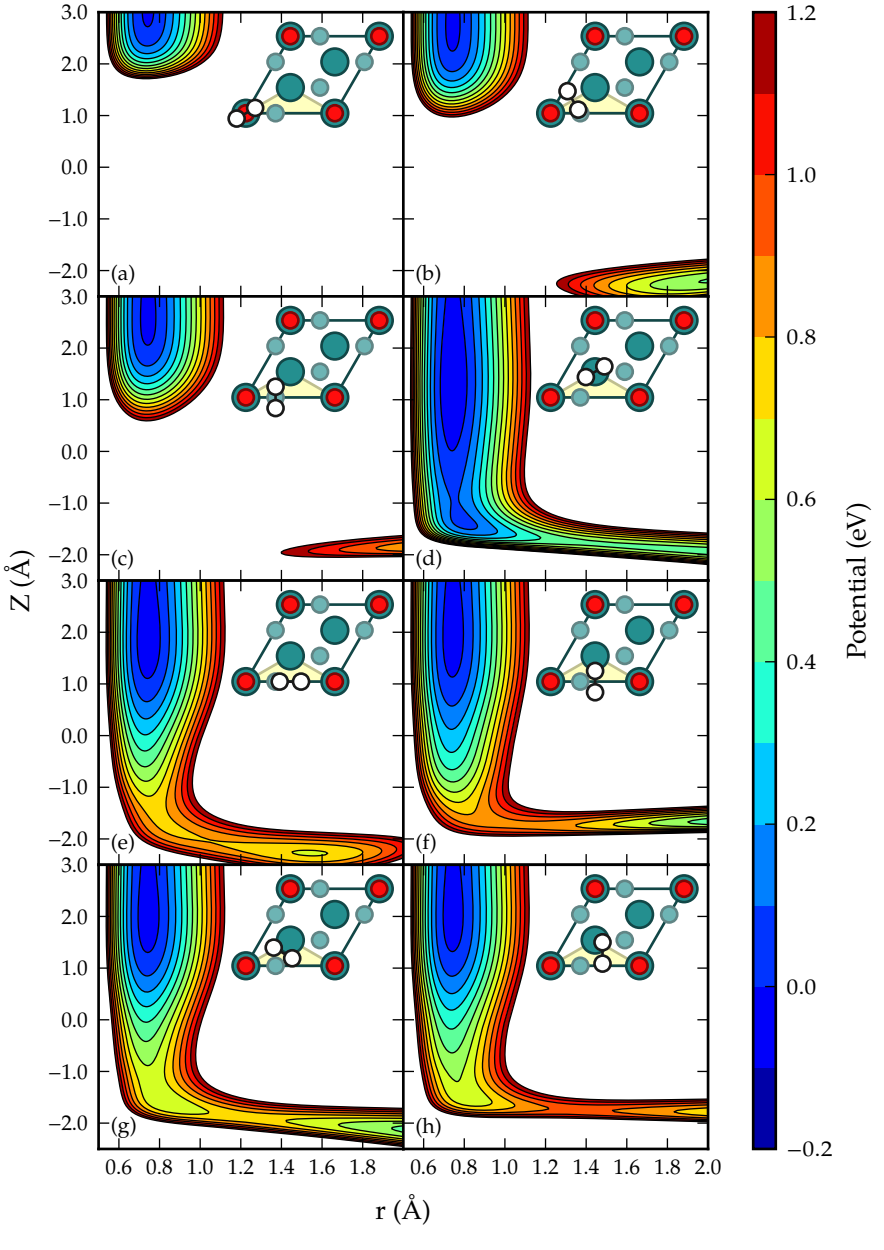

Figure 7.4 The (r, Z) dependence of the PES for H_2 dissociating on 1/3 ML CO-covered Ru(0001) above several different sites and orientations ($\vartheta = 90°$). (a) top_{ads} ($\varphi = 0°$), (b) $\text{bridge}_{\text{ads}}$ ($\varphi = 120°$), (c) hcp ($\varphi = 90°$), (d) top ($\varphi = 0°$), (e) bridge ($\varphi = 0°$), (f) bridge ($\varphi = 90°$), (g) t2h ($\varphi = 150°$), (h) t2f ($\varphi = 90°$).

Table 7.2 Barrier heights and positions for several dissociation geometries for H_2 dissociation on bare and 1/3 ML CO-covered Ru(0001). For all dissociation geometries $\vartheta = 90°$. The notation *a*-to-*b* corresponds to dissociation above the *a* site with the H atoms moving towards the next nearest *b* site. If this notation is ambiguous, the geometry according to figure 7.1(c) is given. The dissociation geometries also considered in figure 7.4 are indicated with the letter of the panel they are shown in. Values for the bare Ru(0001) surface from the PBE-vdW-DF2 PES described in chapter 4. RPBE barrier heights from reference 9.

Site	Surface	r_b (Å)	Z_b (Å)	E_b (eV)	E_b^{RPBE} (eV)
top-to-bridge	bare Ru(0001)	0.751	2.605	0.004	
— on $\mathrm{top_{ads}}$ (a)	CO/Ru(0001)	—	—	—	
— on top (d)	CO/Ru(0001)	0.754	−0.971	0.095	0.30
bridge-to-hollow	bare Ru(0001)	0.796	1.858	0.276	
— on $\mathrm{bridge_{ads}}$ (b)	CO/Ru(0001)	0.773	−0.350	4.347	
— on bridge (e)	CO/Ru(0001)	1.059	−2.050	0.799	0.85
t2h-to-fcc	bare Ru(0001)	0.771	2.139	0.115	
— on $\mathrm{t2h_{ads}}$	CO/Ru(0001)	—	—	—	
— on t2h (g)	CO/Ru(0001)	1.225	−1.887	0.739	
t2f-to-t2f	bare Ru(0001)	1.292	1.552	0.312	
— t2f($\varphi = 90°$) (h)	CO/Ru(0001)	1.312	−1.737	0.923	0.84
— t2f($\varphi = 150°$)	CO/Ru(0001)	0.747	−1.032	0.684	
hcp-to-t2f	bare Ru(0001)	0.850	1.678	0.430	
— hcp($\varphi = 30°$)	CO/Ru(0001)	0.721	−0.538	2.807	
— hcp($\varphi = 90°$) (c)	CO/Ru(0001)	0.741	−0.470	2.389	

CO molecule, dissociation is much more favourable. For all cases in figure 7.4 where a full elbow is shown, late barriers are found. For dissociation directly above the Ru atom without an adsorbed CO molecule, additionally an early barrier and a well are found. This is in general agreement with previous results for the RPBE functional.[9] For bridge-to-hollow dissociation (figure 7.4(e)), however, Groot *et al.* found an early barrier, while here a later barrier is obtained with the use of the PBE-vdW-DF2 functional. For t2f ($\varphi = 90°$) (figure 7.4(h)), only a late barrier is found, whereas previously also an early barrier was found for a geometry, t2f ($\varphi = 88°$), which is close to the one considered here.

In table 7.2 barrier heights and positions for dissociation of H_2 on an ideal 1/3 ML CO-covered Ru(0001) surface ($\sqrt{3} \times \sqrt{3}$ cell) are compared to those for dissociation of H_2 on an ideal, bare Ru(0001) surface. In the case where one geometry for the bare Ru(0001) has multiple symmetry inequivalent geometries for the CO-covered surface due to the addition of CO, both are given. The subscript "ads" refers to the site which is closest to the adsorbed CO molecule (see also figure 7.1). Note that Groot *et al.*[9] only considered the sites furthest away from the CO in their analysis (*i.e.*, the ones here denoted without subscript "ads"). Similar barrier heights are obtained for the fcc and t2f site as for the hcp and t2h site, respectively, and as such, values for a particular orientation are only given for either hcp (t2h) or fcc (t2f). It is clear that for all configurations that are considered the barrier height is increased relative to the bare Ru(0001), and in some cases a particular dissociation geometry even becomes non-dissociative (*i.e.*, no transition state could be found). This is in general agreement with findings obtained using the RPBE functional.[9] The computed barrier heights are in good agreement with previously obtained values[9] with the RPBE functional, except for the top-to-bridge barrier. For this geometry, the PBE-vdW-DF2 functional predicts a barrier height that is 0.20 eV lower than the RPBE barrier height. Note that the barrier referred to is for passage to a local molecular chemisorption minimum, see figure 7.4(d). Sites close to the CO molecule show either a very high barrier (> 2 eV) or no barrier at all.

The results obtained with the PBE-vdW-DF2 functional are at least in qualitative agreement with the results obtained with the RPBE functional.[9] As the dissociation barriers near top_{ads} are very high, it is clear that the H_2 molecule is repelled by the adsorbed CO molecule and dissociation can therefore only occur in the center of the triangles shown in figure 7.2(a), *i.e.*, close to the bare top site. As Z_b near the top site is ≈ -2 Å, it is clear that the H_2 molecule needs to move into the layer of CO molecules, and if needed push the CO molecules aside, in order to be able to dissociate.

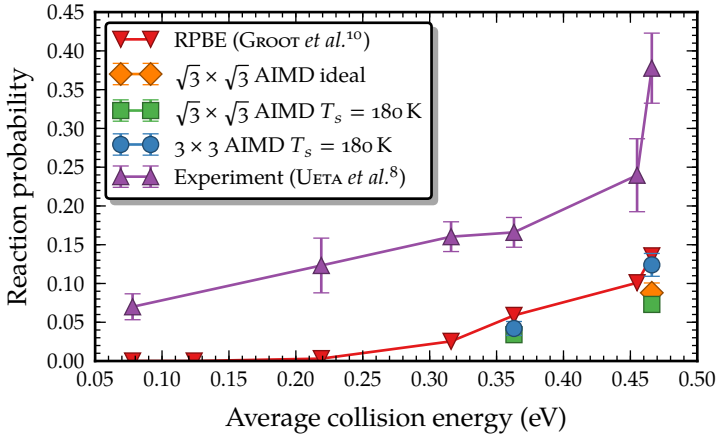

Figure 7.5 Reaction probabilities as a function of average collision energy computed with several methods compared to experiment.[8] Results obtained with the RPBE[57] functional by Groot *et al.*[10] are also shown.

7.3.3 Reaction probability and energy exchange

In figure 7.5 the reaction probability is shown as a function of average collision energy as computed using a rigid, ideal $\sqrt{3} \times \sqrt{3}$ cell, and using $\sqrt{3} \times \sqrt{3}$ and 3×3 simulation cells at $T_s = 180\,\mathrm{K}$. For comparison, the experimental data by Ueta *et al.*[8] and the previous results using the RPBE[57] functional by Groot *et al.*,[9] which were obtained with the use of a rigid, ideal $\sqrt{3} \times \sqrt{3}$ cell in the DFT calculations, are also shown.

It is clear that the PBE-vdW-DF2 reaction probabilities are too low compared to experiment, which was also the case for the previously computed RPBE reaction probabilities.[9] The PBE-vdW-DF2 reaction probabilities are even lower than the RPBE reaction probabilities. The reaction probability computed with a frozen ideal surface matches closely to, or is even slightly larger than, the reaction probability computed with the $\sqrt{3} \times \sqrt{3}$ cell for $T_s = 180\,\mathrm{K}$. The reaction probabilities computed for $T_s = 180\,\mathrm{K}$ are greater if the 3×3 simulation cell is used, this result being statistically significant for $E_{\mathrm{trans}} = 0.466\,\mathrm{eV}$. At this incidence energy, the reaction probability for the 3×3 cell is higher by about 0.05 compared to the $\sqrt{3} \times \sqrt{3}$ cell.

It is not fully understood why a disagreement between theory and

experiment remains. As surface temperature is taken into account here, it seems likely that the disagreement of the PBE-vdW-DF2 reaction probabilities for $T_s = 180$ K with experiment is due to the XC functional not being good enough, even though this functional works well for H_2 dissociation on bare Ru(0001), as shown in chapter 4. Another possible cause for the discrepancy between theory and experiments concerns the coverage of Ru(0001) by CO in the experiment. To obtain the 1/3 ML CO-covered Ru(0001) system, which should correspond to the simple $\sqrt{3}\times\sqrt{3}$ system studied here,[15,19,21,22] the experiments worked with a system exhibiting half the measured saturation coverage.[8] The assumption has been that this should correspond to the 1/3 ML covered surface, because the saturation coverage is experimentally known to be 2/3 ML.[35] If the saturation coverage achieved by Ueta *et al.* however was somehow less than 2/3 ML, this could explain the observed discrepancy with experiment at least in part. Specifically, on average the coverage should then be less than 1/3 ML in the molecular beam experiment, and that should make the measured reactivity higher than the one calculated here. This could be aggravated by inhomogeneity effects, as this could give rise to the formation of islands[21] with the 1/3 ML $\sqrt{3} \times \sqrt{3}$ coverage considered here and areas with a much lower coverage, which should exhibit a much greater reactivity. It would therefore be useful if the experiments could be repeated with the accompanying use of low-energy electron diffraction (LEED) to ascertain the surface coverage pattern used in the experiments indeed corresponds to the $\sqrt{3}\times\sqrt{3}$ pattern considered here, to rule out this source of error.

The remainder of this section will focus on the effects motion of the surface has on the reaction probability. Possible reasons for why the reaction probability of D_2 on a thermal slab might be slightly smaller than the reaction probability of D_2 on a frozen ideal slab, as found with the $\sqrt{3}\times\sqrt{3}$ cell, are that the CO molecules and the Ru(0001) surface act as an energy sink, causing the D_2 to lose energy it could otherwise have used to overcome the barrier to dissociation, and that slightly less of the surface might be available because the CO molecule is, on average, slightly tilted in the dynamics. From the present results, it is not clear how important these effects are.

With respect to the difference between the smaller and larger simu-

Table 7.3 For all AIMD calculations, the average initial translational energy of the molecules that go on to react, along with the reaction probability for that calculation.

Energy	Cell model	$\langle E_{\text{trans}} \rangle_{\text{react}}$ (eV)	P_r
0.363 eV	$(\sqrt{3} \times \sqrt{3})$ 180 K	0.415 ± 0.015	0.034 ± 0.008
	(3×3) 180 K	0.452 ± 0.028	0.042 ± 0.009
0.466 eV	$(\sqrt{3} \times \sqrt{3})$ ideal	0.607 ± 0.020	0.088 ± 0.013
	$(\sqrt{3} \times \sqrt{3})$ 180 K	0.585 ± 0.016	0.073 ± 0.008
	(3×3) 180 K	0.576 ± 0.020	0.124 ± 0.015

lation cell, it is not immediately apparent what could be the cause. Possible causes could be extra dynamical effects due to the presence of multiple independent CO molecules, such as extra possibilities for energy exchange, but also small differences in DFT parameters (a smaller k-grid was used for the 3×3 calculations) might play a role. These two effects are discussed below. As is shown below, the larger reactivity obtained with the 3×3 cell is probably due to the D_2 exchanging energy with three independent CO molecules, which allows the nearby CO molecules to move apart, so that the reactive Ru(0001) surface becomes exposed.

Convergence tests have been carried out on the k-point grid used for the DFT calculations. From these convergence tests, it is clear that the H_2/CO+Ru(0001) interaction is described accurately, the largest observed difference between the $\sqrt{3} \times \sqrt{3}$ cell and the 3×3 cell being about 34 meV. Although this number is not small on the scale of the differences (the relative displacement on the energy scale of the two $T_s = 180$ K reaction probability curves is estimated to be in the range of $50 - 100$ meV), it cannot explain the whole difference. Also, the maximum observed energy difference was in the opposite direction to that which would be expected to explain the difference in reactivity (the potential near the surface was higher for the 3×3 cell rather than lower, which decreases reactivity instead of increasing it). It therefore seems unlikely that small differences in the DFT parameters can explain the observed differences for the two simulation cells.

In table 7.3 the average initial translational energy of the molecules that go on to react is shown for all AIMD calculations, together with

the reaction probability for each calculation. It is clear that for the different simulation cell models the average initial translational energy of the dissociating molecules is the same, at least insofar as the error due to sampling is concerned. This suggests that the "effective" barriers to dissociation are the same for all different simulation cell sizes and thus that differences between the models are not due to static effects (*i.e.*, due to the barrier to dissociation being different for different sizes of the simulation cell).

In table 7.1 several geometrical properties are given of the surface, with D_2 (the dynamics done to determine the reaction probability) and without D_2 (the dynamics of the slab used to generate initial conditions). In section 7.3.1 the results without D_2 were discussed. The results with D_2, and the comparison to the results without D_2, are discussed here. The numbers in table 7.1 correspond to averages from the trajectories beginning with the D_2 molecule in the gas phase, for the case that D_2 is present. As such, these parameters do not straightforwardly correspond to a physically measurable situation, and these parameters are only used to compare to the (in principle measurable) parameters for the case without D_2. For both the $\sqrt{3} \times \sqrt{3}$ and the 3×3 cell, the mean square displacement of the C and O atoms is increased markedly compared to the case without D_2, and even more so for the 3×3 cell than for the $\sqrt{3} \times \sqrt{3}$ cell. This occurs for both the parallel and perpendicular components of the displacements, but mostly for the parallel component. Intriguingly, for the perpendicular component, little or no difference is found between the $\sqrt{3} \times \sqrt{3}$ and the 3×3 cells, whereas the parallel component does show a difference. Furthermore, the average tilt angles of the CO with respect to the surface are also increased. This means that the geometry of the CO-covered Ru(0001) surface is altered by the impinging D_2 molecules, and more so for the 3×3 cell than for the $\sqrt{3} \times \sqrt{3}$ cell. As energy in D_2 can be exchanged with the surface to alter the geometry of the CO-covered surface, this in turn suggests that more energy is exchanged with the surface for the 3×3 cell than for the $\sqrt{3} \times \sqrt{3}$ cell. In particular, the O atom moves most, with the C atom moving less, as also indicated by the increased tilt angles. The other parameters, *i.e.*, the interlayer spacing, the protrusion of the topmost Ru atom, the Ru–C and C–O bond lengths are all not much influenced

Table 7.4 Amount of energy exchanged with the surface in collisions of D_2 with the CO-covered Ru(0001) surface, for cases which result in scattering. Direct trajectories make only a single rebound.

Energy	$\sqrt{3} \times \sqrt{3}$ cell (eV)	3×3 cell (eV)
0.363 eV	0.080 ± 0.003	0.191 ± 0.005
— direct only	0.077 ± 0.003	0.187 ± 0.005
— indirect only	0.106 ± 0.013	0.225 ± 0.018
0.466 eV	0.105 ± 0.002	0.263 ± 0.007
— direct only	0.104 ± 0.002	0.258 ± 0.008
— indirect only	0.119 ± 0.010	0.278 ± 0.014

by the impinging D_2 molecule. These results therefore indicate that energy can be exchanged between D_2 and the CO molecules, and not so much with the Ru(0001) surface.

In table 7.4 the amount of energy exchange of the molecule with the surface is shown for scattered trajectories, which is defined as the total energy lost to the surface by the D_2 molecule at $t = t_{\text{final}}$ compared to $t = 0$. The results have also been split into direct (single rebound) and indirect (multiple rebounds) scattering. It is clear that the amount of energy exchanged in the larger simulation cell is significantly larger than that for the smaller simulation cell, by about a factor 2.5 for the higher incidence energy and slightly less for the lower incidence energy. The number of atoms has increased by a factor 3 on going from the smaller to the larger cell, which suggests that, for the atoms with which energy is exchanged, also energy is exchanged with molecules that would correspond to mirror images in the $\sqrt{3} \times \sqrt{3}$ cell, but are independent in the 3×3 cell. For indirect scattering, slightly more energy is exchanged than is the case for direct scattering.

Intriguingly, a considerable amount of energy is transferred to the surface for both simulation cell sizes. It is rather remarkable that in the case of the 3×3 cell the amount of energy that is exchanged is over half the amount of initial translational energy, in particular if this is compared to the amount for the $\sqrt{3} \times \sqrt{3}$ cell. A likely explanation for this discrepancy seems to be that the D_2 molecule deposits energy into the CO molecule(s). It is interesting to see that in spite of the large energy

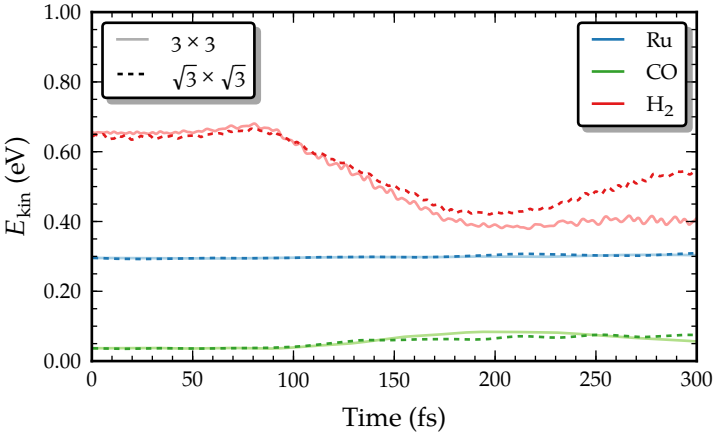

Figure 7.6 Time evolution of the kinetic energy of the ruthenium slab, the CO molecules and H_2 molecule, averaged over all trajectories with $t_{final} > 300$ fs, for the $\sqrt{3}\times\sqrt{3}$ and 3×3 cells. The energies for the CO and Ru atoms have been normalized to the amount present in the $\sqrt{3}\times\sqrt{3}$ cell.

transfer to the CO molecule(s) the reaction probability of the ideal and the $T_s = 180$ K surface do not differ much. This suggests that the energy transfer is at least partly compensated by new reaction pathways becoming available.

To better understand to what part of the surface the energy is lost, in figure 7.6 the time evolution of the kinetic energy of the ruthenium slab, the CO molecules and the H_2 molecule, averaged over all trajectories with $t_{final} > 300$ fs, is shown. The kinetic energies of the CO molecules and Ru atoms for the 3×3 cell have been divided by three to account for the increase in the number of atoms in the 3×3 cell compared to the $\sqrt{3} \times \sqrt{3}$ cell. It is clear that the amount of kinetic energy that is transferred to the Ru atoms is rather small, while the amount of kinetic energy that is transferred to the CO molecules is larger. No large differences are observed between the smaller and larger cell. These results therefore show that energy is indeed exchanged with the, in the 3×3 cell, independent images, and, in particular, with the CO molecules.

Further information about the differences between the $\sqrt{3} \times \sqrt{3}$ and 3×3 cell can be found by binning the energy that is exchanged with the

Table 7.5 Amount of energy exchanged with the surface in collisions of D_2 with the CO-covered Ru(0001) surface, binned with respect to the impact site.

Energy	Site	$\sqrt{3}\times\sqrt{3}$ cell (eV)	3×3 cell (eV)
0.363 eV	top_{ads}	0.102 ± 0.008	0.104 ± 0.009
	top	0.056 ± 0.007	0.203 ± 0.013
	$bridge_{ads}$	0.100 ± 0.005	0.173 ± 0.009
	bridge	0.057 ± 0.004	0.255 ± 0.013
	hcp/fcc	0.080 ± 0.005	0.215 ± 0.010
0.466 eV	top_{ads}	0.167 ± 0.009	0.178 ± 0.012
	top	0.066 ± 0.005	0.269 ± 0.017
	$bridge_{ads}$	0.111 ± 0.003	0.222 ± 0.011
	bridge	0.095 ± 0.007	0.329 ± 0.014
	hcp/fcc	0.099 ± 0.004	0.295 ± 0.013

surface with respect to the impact site of the molecule. The results of such an analysis are given in table 7.5 and the bins that have been used are indicated in figure 7.2(b). For all sites that are considered, except the top_{ads} site, and both incidence energies, the amount of energy exchange is larger for the 3×3 cell than for the $\sqrt{3}\times\sqrt{3}$ cell. For the top_{ads} site however, the amount of energy exchange is, to within the statistical errors indicated, the same for both simulation cells. As the top_{ads} site corresponds to the D_2 molecule colliding directly on top of the CO molecule, this difference is not surprising, because the next CO molecule is $\sqrt{3}$ times the Ru–Ru distance away, which for the present case is 4.77 Å. The molecule thus exchanges energy with only a single CO molecule, and predominantly energy in motion in the Z direction, as it is a head-on collision and the molecule initially only has momentum in Z. For all other sites, the interpretation is that the molecule will go in between the CO molecules, which means that the D_2 molecule may be able to exchange energy with up to three nearest CO molecules. In this case, energy exchange will mostly involve motion in the U and V directions, as the D_2 molecule collides with the CO molecule(s) more from the side. As in the $\sqrt{3}\times\sqrt{3}$ cell only a single CO molecule is present the D_2 molecule pushes against its mirror images in such a way that the forces parallel to the surface partially cancel each other. As in the 3×3 cell

three independent CO molecules are present for similarly small D_2–CO distances projected on the surface (see figure 7.2(a)), such a cancellation of forces does not occur and energy can be exchanged with all of the three independent CO molecules without forces between CO and D_2 being partly cancelled through the imposed periodicity, explaining the larger energy exchange.

If energy is exchanged between the D_2 and CO in the U and V directions, the CO will move along the surface, but in case of the $\sqrt{3} \times \sqrt{3}$ cell the entire layer moves, as only a single independent CO molecule is present. In case of the 3×3 cell however, the three independent CO molecules may move apart. This can be analysed by tracking the size of the 2D triangles that are spanned by the CO molecules (six for the 3×3 cell, see also figure 7.2(a)). In table 7.6 the size of the surface triangle in which the D_2 is initially located ($t = 0$) is shown for the first and final time step of both reactive and non-reactive trajectories, with the corners of the triangle attached to either the C or the O atoms. For both non-reactive and reactive trajectories, and for both the C and O triangles, the size of the surface triangle in which the D_2 is initially located grows during the dynamics, from a value essentially equal to that of an ideal triangle size to a value which is in the range of about 15% to 30% larger, *i.e.*, the CO layer locally "opens" due to the impinging D_2 molecule pushing the CO molecules aside. The O triangles are larger than the C triangles, suggesting that the molecules, apart from being pushed away, are also tilted away to make room for D_2. As the initial triangle size is slightly larger for dissociative trajectories than for scattered trajectories, an additional effect appears to be that in the 3×3 CO-covered surface the D_2 molecule can find spots where the CO molecules have already moved apart a bit, which opens the surface to reaction. It should, however, be stressed that such an effect is small and not fully established at present due to the limited statistics of the dynamics calculations. The main established mechanism therefore is the CO layer opening effect due to the impinging D_2 molecule pushing the CO molecules away.

The difference between the reaction probability of the 3×3 and the $\sqrt{3} \times \sqrt{3}$ cells can thus be explained mainly from the amount of energy exchanged between the D_2 molecule and the surface, and in particular energy transferred to motion of CO molecules parallel to the surface.

Energy	Δ_C (Å²)		Δ_O (Å²)	
	$t = 0$	$t = t_{final}$	$t = 0$	$t = t_{final}$
0.363 eV	9.92 ± 0.03	11.29 ± 0.08	10.04 ± 0.05	12.32 ± 0.13
— scattering	9.91 ± 0.03	11.26 ± 0.08	10.03 ± 0.05	12.29 ± 0.14
— dissociation	9.97 ± 0.13	11.92 ± 0.18	10.22 ± 0.27	12.75 ± 0.30
0.466 eV	9.85 ± 0.03	11.56 ± 0.08	9.94 ± 0.05	12.67 ± 0.14
— scattering	9.83 ± 0.03	11.45 ± 0.09	9.90 ± 0.05	12.61 ± 0.16
— dissociation	10.03 ± 0.09	12.26 ± 0.17	10.21 ± 0.15	13.05 ± 0.30
ideal	9.85	—	9.85	—

Table 7.6 Size of the surface triangle (see figure 7.2(a)) in which the D_2 is initially located for D_2 scattering or dissociation on the CO-covered Ru(0001) surface. t_{final} is taken to be the first time step for which the analysis conditions are met.

CHAPTER 7

Ab initio molecular dynamics study of D_2 dissociation on CO-precovered Ru(0001)

Significantly more energy is exchanged between the molecule and the CO overlayer for the 3×3 cell than for the $\sqrt{3} \times \sqrt{3}$ cell. As a result of this, the CO molecules can move away from one another in the 3×3 cell. Only in the 3×3 cell (three) independent CO molecules are present. These independent CO molecules can move apart, leaving more space, and therefore more favourable pathways to reaction, for the molecule.

An interesting open question is whether or not further increasing the size of the simulation cell could result in further changes in the reaction probability. As the spacing between different CO molecules is rather large (the diagonal of the HCP(0001) unit cell which, for this system, is 4.77 Å), it seems likely that the D_2 molecule cannot influence the motion of the next nearest neighbour CO molecule, meaning CO molecules further away than the three making up the triangle in which it lands (see figure 7.2). It is therefore not expected that increasing the size of the simulation cell further will dramatically change the reaction probability.

Even though the PBE-vdW-DF2 functional used here describes the reaction of H_2 and D_2 on bare Ru(0001) rather well (chapter 4), it severely underestimates the reactivity of D_2 on CO-covered Ru(0001). The PBE-vdW-DF2 functional may be described as a candidate SRP XC functional for H_2/Ru(0001) (it described the dissociation of H_2 and D_2 quite well, but its validity for other (diffraction) experiments was not established). The present study suggests that a XC functional that gives a good description of H_2 reacting on a bare metal surface may not necessarily work for the same metal, but with the surface poisoned by CO. Additional studies on other H_2–metal surface and H_2–CO pre-covered metal surface systems are needed to establish whether this finding is general to these systems and what causes the problem noted.

7.4 Conclusions

The dissociation of D_2 on 1/3 ML CO-covered Ru(0001) has been studied with quasi-classical AIMD calculations using the PBE-vdW-DF2 functional. The PBE-vdW-DF2 functional gives a reasonable description of the structure of the CO-covered surface, both compared to experimental data and compared to previous theoretical studies. The

molecule–surface interaction of D_2 with the CO-covered Ru(0001) surface is mostly in agreement with a previous study[9] where the RPBE functional was used, but some qualitative as well as quantitative differences are found.

The reaction probabilities computed with the AIMD method are not in agreement with experimental data, as the computed reaction probabilities are too low. The reaction probabilities are however in reasonable agreement with the previous RPBE results using a frozen ideal surface model, although the values reported here are still slightly lower. The discrepancy with experimental data is assigned to the functional which is used here not working well enough for this system, in spite of the fact that it works well for H_2 dissociation on bare Ru(0001). For the higher investigated incidence energy ($E_{\text{trans}} = 0.466\,\text{eV}$), the reaction probability for the 3×3 cell is somewhat higher (by about 0.05) than for the $\sqrt{3} \times \sqrt{3}$ cell.

The reaction probability for D_2 on a $T_s = 180\,\text{K}$ slab is overall similar to the reaction probability for D_2 on an ideal slab. This arises due to a balance between opposing factors. The D_2 molecule loses a rather large amount of energy to the surface. In this way the impinging D_2 molecules can push aside the CO molecule(s). Although the resulting energy loss leads to a decrease in reaction, as this energy cannot be used to overcome the barrier to reaction, the displacement of CO molecules leads to new reactive pathways opening up. The CO molecules in a $T_s = 180\,\text{K}$ slab are additionally slightly tilted, whereas they are upright in the ideal slab, which may lead to a decrease of reactivity, although the size of this effect is not clear from the present results.

The difference between the reaction probabilities obtained for the higher incidence energy for the $\sqrt{3} \times \sqrt{3}$ and the 3×3 cells can be explained by the number of independently moving CO molecules present in the cell. For the 3×3 cell, the D_2 molecule can exchange energy with up to three independent CO molecules, allowing the CO layer of the surface to open up locally. For the $\sqrt{3} \times \sqrt{3}$ cell only a single independent CO molecule is present, which leads to some of the forces working on the C and O atoms to be cancelled out due to the D_2 molecule pushing different mirror images of these atoms in opposing directions. As a result, the D_2 molecule exchanges less energy with the surface and cannot

displace the CO molecules far enough for dissociation to become more effective.

References

[1] G. J. Kroes and C. Díaz. Quantum and classical dynamics of reactive scattering of H_2 from metal surfaces. Accepted to *Chemical Society Reviews*. doi: 10.1039/C5CS00336A. 2016.

[2] A. Gross and A. Dianat. Hydrogen dissociation dynamics on precovered Pd surfaces: Langmuir is still right. *Physical Review Letters* **98**(20), 206107, 2007.

[3] A. Lozano, A. Gross, and H. F. Busnengo. Adsorption dynamics of H_2 on Pd(100) from first principles. *Physical Chemistry Chemical Physics* **11**(27), pp. 5814–5822, 2009.

[4] A. Gross. *Ab initio* molecular dynamics simulations of the adsorption of H_2 on palladium surfaces. *ChemPhysChem* **11**(7), pp. 1374–1381, 2010.

[5] A. Lozano, A. Gross, and H. F. Busnengo. Molecular dynamics study of H_2 dissociation on H-covered Pd(100). *Physical Review B* **81**(12), 121402, 2010.

[6] A. Gross. Coverage effects in the adsorption of H_2 on Pd(100) studied by *ab initio* molecular dynamics simulations. *Journal of Chemical Physics* **135**(17), 174707, 2011.

[7] A. Gross. *Ab initio* molecular dynamics study of H_2 adsorption on sulfur- and chlorine-covered Pd(100). *Surface Science* **608**, pp. 249–254, 2013.

[8] H. Ueta, I. M. N. Groot, M. A. Gleeson, S. Stolte, G. C. McBane, L. B. F. Juurlink, and A. W. Kleyn. CO blocking of D_2 dissociative adsorption on Ru(0001). *ChemPhysChem* **9**(16), pp. 2372–2378, 2008.

[9] I. M. N. Groot, J. C. Juanes-Marcos, R. A. Olsen, and G. J. Kroes. A theoretical study of H_2 dissociation on $(\sqrt{3}x\sqrt{3})R30^\circ$ CO/Ru(0001). *Journal of Chemical Physics* **132**(14), 144704, 2010.

[10] I. M. N. Groot, J. C. Juanes-Marcos, C. Díaz, M. F. Somers, R. A. Olsen, and G. J. Kroes. Dynamics of dissociative adsorption of hydrogen on a CO-precovered Ru(0001) surface: a comparison of theoretical and experimental results. *Physical Chemistry Chemical Physics* **12**(6), pp. 1331–1340, 2010.

[11] B. Baule. Theoretische Behandlung der Erscheinungen in verdünnten Gasen. *Annalen der Physik* **349**(9), pp. 145–176, 1914.

[12] A. Gross. *Theoretical Surface Science*. Berlin: Springer, 2003.

[13] P. Zhao, Y. He, D. B. Cao, X. Wen, H. Xiang, Y. W. Li, J. Wang, and H. Jiao. High coverage adsorption and co-adsorption of CO and H_2 on Ru(0001) from DFT and thermodynamics. *Physical Chemistry Chemical Physics* **17**(29), pp. 19446–19456, 2015.

[14] J. C. Fuggle, T. E. Madey, M. Steinkilberg, and D. Menzel. Photoelectron spectroscopic studies of adsorption of CO and oxygen on Ru(001). *Surface Science* **52**(3), pp. 521–541, 1975.

[15] G. Michalk, W. Moritz, H. Pfnür, and D. Menzel. A LEED determination of the structures of Ru(001) and of CO/Ru(001)–$\sqrt{3} \times \sqrt{3}$R30°. *Surface Science* **129**(1), pp. 92–106, 1983.

[16] M. Gierer, H. Bludau, H. Over, and G. Ertl. The bending mode vibration of CO on Ru(0001) studied with low-energy electron-diffraction. *Surface Science* **346**(1–3), pp. 64–72, 1996.

[17] J. C. Fuggle, M. Steinkilberg, and D. Menzel. Angular dependence of UV photoemission spectra from clean Ru(001) and from adsorbed oxygen and CO. *Chemical Physics* **11**(2), pp. 307–317, 1975.

[18] T. E. Madey. The geometry of CO on Ru(001): Evidence for bending vibrations in adsorbed molecules. *Surface Science* **79**(2), pp. 575–588, 1979.

[19] E. D. Williams and W. H. Weinberg. Geometric structure of carbon monoxide chemisorbed on the ruthenium (001) surface at low temperatures. *Surface Science* **82**(1), pp. 93–101, 1979.

[20] H. Pfnür, D. Menzel, F. M. Hoffmann, A. Ortega, and A. M. Bradshaw. High resolution vibrational spectroscopy of CO on Ru(001): The importance of lateral interactions. *Surface Science* **93**(2–3), pp. 431–452, 1980.

[21] H. Pfnür and D. Menzel. Lateral interactions for CO/Ru(001): order-disorder transitions of the $\sqrt{3}$ structure. *Surface Science* **148**(2–3), pp. 411–438, 1984.

[22] H. Pfnür and H. J. Heier. Order-disorder phenomena in the system CO/Ru(001). *Berichte der Bunsengesellschaft für physikalische Chemie* **90**(3), pp. 272–277, 1986.

[23] H. Pfnür and D. Menzel. The influence of adsorbate interactions on kinetics and equilibrium for CO on Ru(001). I. Adsorption kinetics. *Journal of Chemical Physics* **79**(5), pp. 2400–2410, 1983.

[24] H. Pfnür, P. Feulner, H. A. Engelhardt, and D. Menzel. An example of "fast" desorption: anomalously high pre-exponentials for CO desorption from Ru(001). *Chemical Physics Letters* **59**(3), pp. 481–486, 1978.

[25] H. Pfnür, P. Feulner, and D. Menzel. The influence of adsorbate interactions on kinetics and equilibrium for CO on Ru(001). II. Desorption kinetics and equilibrium. *Journal of Chemical Physics* **79**(9), pp. 4613–4623, 1983.

[26] J. Braun, K. L. Kostov, G. Witte, and C. Woll. CO overlayers on Ru(0001) studied by helium atom scattering: structure, dynamics, and the influence of coadsorbed H and O. *Journal of Chemical Physics* **106**(19), pp. 8262–8273, 1997.

[27] H. Over, W. Moritz, and G. Ertl. Anisotropic atomic motions in structural analysis by low energy electron diffraction. *Physical Review Letters* **70**(3), pp. 315–318, 1993.

[28] H. Over, M. Gierer, H. Bludau, and G. Ertl. Anisotropic thermal displacements of adsorbed atoms and molecules on surfaces studied by low-energy electron diffraction. *Physical Review B* **52**(23), pp. 16812–16829, 1995.

[29] M. Bonn, S. Funk, Ch. Hess, D. N. Denzler, C. Stampfl, M. Scheffler, M. Wolf, and G. Ertl. Phonon- versus electron-mediated desorption and oxidation of CO on Ru(0001). *Science* **285**(5430), pp. 1042–1045, 1999.

[30] L. Diekhöner, H. Mortensen, A. Baurichter, and A. C. Luntz. Laser assisted associative desorption of N_2 and CO from Ru(0001). *Journal of Chemical Physics* **115**(7), pp. 3356–3373, 2001.

[31] J. Gladh, T. Hansson, and H. Öström. Electron- and phonon-coupling in femtosecond laser-induced desorption of CO from Ru(0001). *Surface Science* **615**, pp. 65–71, 2013.

[32] C. Hess, S. Funk, M. Bonn, D. N. Denzler, M. Wolf, and G. Ertl. Femtosecond dynamics of chemical reactions at surfaces. *Applied Physics A* **71**(5), pp. 477–483, 2000.

[33] P. Jakob. Fermi resonance distortion of the Ru–CO stretching mode of CO adsorbed on Ru(001). *Journal of Chemical Physics* **108**(12), pp. 5035–5043, 1998.

[34] K. L. Kostov, H. Rauscher, and D. Menzel. Adsorption of CO on oxygen-covered Ru(001). *Surface Science* **278**(1–2), pp. 62–86, 1992.

[35] D. E. Starr and H. Bluhm. CO adsorption and dissociation on Ru(0001) at elevated pressures. *Surface Science* **608**, pp. 241–248, 2013.

[36] S. Wagner, H. Öström, A. Kaebe, M. Krenz, M. Wolf, A. C. Luntz, and C. Frischkorn. Activated associative desorption of C + O → CO from Ru(001) induced by femtosecond laser pulses. *New Journal of Physics* **10**(12), 125031, 2008.

[37] S. Wurm, P. Feulner, and D. Menzel. Extremely high vibrational excitation of CO molecules desorbed from transition metal surfaces by electron impact. *Physical Review Letters* **74**(13), pp. 2591–2594, 1995.

[38] H. Öström, H. Öberg, H. Xin, J. LaRue, M. Beye, M. Dell'Angela, J. Gladh, M. L. Ng, J. A. Sellberg, S. Kaya, G. Mercurio, D. Nordlund, M. Hantschmann, F. Hieke, D. Kühn, W. F. Schlotter, G. L. Dakovski, J. J. Turner, M. P. Minitti, A. Mitra, S. P. Moeller, A. Föhlisch, M. Wolf, W. Wurth, M. Persson, J. K. Nørskov, F. Abild-Pedersen, H. Ogasawara, L. G. M. Pettersson, and A. Nilsson. Probing the transition state region in catalytic CO oxidation on Ru. *Science* **347**(6225), pp. 978–982, 2015.

[39] M. Dell'Angela, T. Anniyev, M. Beye, R. Coffee, A. Föhlisch, J. Gladh, T. Katayama, S. Kaya, O. Krupin, J. LaRue, A. Møgelhøj, D. Nordlund, J. K. Nørskov, H. Öberg, H. Ogasawara, H. Öström, L. G. M. Pettersson, W. F. Schlotter, J. A. Sellberg, F. Sorgenfrei, J. J. Turner, M. Wolf, W. Wurth, and A. Nilsson. Real-time observation of surface bond breaking with an X-ray laser. *Science* **339**(6125), pp. 1302–1305, 2013.

[40] I. M. Ciobica and R. A. van Santen. Carbon monoxide dissociation on planar and stepped Ru(0001) surfaces. *Journal of Physical Chemistry B* **107**(16), pp. 3808–3812, 2003.

[41] I. M. Ciobica, A. W. Kleyn, and R. A. van Santen. Adsorption and coadsorption of CO and H on ruthenium surfaces. *Journal of Physical Chemistry B* **107**(1), pp. 164–172, 2003.

[42] M. Gajdos, A. Eichler, and J. Hafner. CO adsorption on close-packed transition and noble metal surfaces: trends from *ab initio* calculations. *Journal of Physics: Condensed Matter* **16**(8), pp. 1141–1164, 2004.

[43] J. J. Mortensen, Y. Morikawa, B. Hammer, and J. K. Nørskov. A comparison of N_2 and CO adsorption on Ru(001). *Zeitschrift für Physikalische Chemie* **198**(1–2), pp. 113–122, 1997.

[44] C. Stampfl and M. Scheffler. Energy barriers and chemical properties in the coadsorption of carbon monoxide and oxygen on Ru(0001). *Physical Review B* **65**(15), 155417, 2002.

[45] J. S. McEwen and A. Eichler. Phase diagram and adsorption-desorption kinetics of CO on Ru(0001) from first principles. *Journal of Chemical Physics* **126**(9), 094701, 2007.

[46] A. Stroppa and G. Kresse. The shortcomings of semi-local and hybrid functionals: what we can learn from surface science studies. *New Journal of Physics* **10**(6), 063020, 2008.

[47] B. Hammer, Y. Morikawa, and J. K. Nørskov. CO chemisorption at metal surfaces and overlayers. *Physical Review Letters* **76**(12), pp. 2141–2144, 1996.

[48] F. Abild-Pedersen and M. P. Andersson. CO adsorption energies on metals with correction for high coordination adsorption sites – a density functional study. *Surface Science* **601**(7), pp. 1747–1753, 2007.

[49] J. Sun, M. Marsman, A. Ruzsinszky, G. Kresse, and J. P. Perdew. Improved lattice constants, surface energies, and CO desorption energies from a semilocal density functional. *Physical Review B* **83**(12), 121410(R), 2011.

[50] C. Corriol, G. R. Darling, S. Holloway, I. Andrianov, T. Klamroth, and P. Saalfrank. Vibrational heating in electron stimulated desorption of CO from transition metals: a classical mechanics analysis. *Surface Science* **528**(1–3), pp. 27–34, 2003.

[51] C. Corriol, G. R. Darling, S. Holloway, W. Brenig, I. Andrianov, T. Klamroth, and P. Saalfrank. Theory of electron stimulated desorption and dissociation of CO at transition metals. *Journal of Chemical Physics* **117**(9), pp. 4489–4498, 2002.

[52] G. Füchsel, J. C. Tremblay, and P. Saalfrank. A six-dimensional potential energy surface for Ru(0001)(2×2):CO. *Journal of Chemical Physics* **141**(9), 094704, 2014.

[53] I. M. N. Groot, H. Ueta, M. J. T. C. van der Niet, A. W. Kleyn, and L. B. F. Juurlink. Supersonic molecular beam studies of dissociative adsorption of H_2 on Ru(0001). *Journal of Chemical Physics* **127**(24), 244701, 2007.

[54] P. Nieto, D. Farías, R. Miranda, M. Luppi, E. J. Baerends, M. F. Somers, M. J. T. C. van der Niet, R. A. Olsen, and G. J. Kroes. Diffractive and reactive scattering of H_2 from Ru(0001): experimental and theoretical study. *Physical Chemistry Chemical Physics* **13**(18), pp. 8583–8597, 2011.

[55] J. P. Perdew, J. A. Chevary, S. H. Vosko, K. A. Jackson, M. R. Pederson, D. J. Singh, and C. Fiolhais. Atoms, molecules, solids, and surfaces: applications of the generalized gradient approximation for exchange and correlation. *Physical Review B* **46**(11), pp. 6671–6687, 1992.

[56] J. P. Perdew, K. Burke, and M. Ernzerhof. Generalized gradient approximation made simple. *Physical Review Letters* **77**(18), pp. 3865–3868, 1996.

[57] B. Hammer, L. B. Hansen, and J. K. Nørskov. Improved adsorption energetics within density-functional theory using revised Perdew-Burke-Ernzerhof functionals. *Physical Review B* **59**(11), pp. 7413–7421, 1999.

[58] C. Díaz, E. Pijper, R. A. Olsen, H. F. Busnengo, D. J. Auerbach, and G. J. Kroes. Chemically accurate simulation of a prototypical surface reaction: H_2 dissociation on Cu(111). *Science* **326**(5954), pp. 832–834, 2009.

[59] M. Dion, H. Rydberg, E. Schröder, D. C. Langreth, and B. I. Lundqvist. Van der Waals density functional for general geometries. *Physical Review Letters* **92**(24), 246401, 2004.

[60] K. Lee, E. D. Murray, L. Kong, B. I. Lundqvist, and D. C. Langreth. Higher-accuracy van der Waals density functional. *Physical Review B* **82**(8), 081101, 2010.

[61] P. J. Feibelman, B. Hammer, J. K. Nørskov, F. Wagner, M. Scheffler, R. Stumpf, R. Watwe, and J. Dumesic. The CO/Pt(111) puzzle. *Journal of Physical Chemistry B* **105**(18), pp. 4018–4025, 2001.

[62] A. Stroppa, K. Termentzidis, J. Paier, G. Kresse, and J. Hafner. CO adsorption on metal surfaces: a hybrid functional study with plane-wave basis set. *Physical Review B* **76**(19), 195440, 2007.

[63] L. Schimka, J. Harl, A. Stroppa, A. Grüneis, M. Marsman, F. Mittendorfer, and G. Kresse. Accurate surface and adsorption energies from many-body perturbation theory. *Nature Materials* **9**(9), pp. 741–744, 2010.

[64] P. Lazić, M. Alaei, N. Atodiresei, V. Caciuc, R. Brako, and S. Blügel. Density functional theory with nonlocal correlation: a key to the solution of the CO adsorption puzzle. *Physical Review B* **81**(4), 045401, 2010.

[65] G. J. Kroes. Towards chemically accurate simulation of molecule-surface reactions. *Physical Chemistry Chemical Physics* **14**(43), pp. 14966–14981, 2012.

[66] M. Born and R. Oppenheimer. Zur Quantentheorie der Molekeln. *Annalen der Physik* **389**(20), pp. 457–484, 1927.

[67] W. Kohn and L. J. Sham. Self-consistent equations including exchange and correlation effects. *Physical Review* **140**(4A), A1133–A1138, 1965.

[68] P. Hohenberg and W. Kohn. Inhomogeneous electron gas. *Physical Review* **136**(3B), B864–B871, 1964.

[69] C. C. Marston and G. G. Balint-Kurti. The Fourier grid Hamiltonian method for bound state eigenvalues and eigenfunctions. *Journal of Chemical Physics* **91**(6), pp. 3571–3576, 1989.

[70] J. W. Arblaster. Crystallographic properties of ruthenium. *Platinum Metals Review* **56**(3), pp. 181–189, 2013.

[71] G. Kresse and J. Hafner. *Ab initio* molecular dynamics for liquid metals. *Physical Review B* **47**(1), pp. 558–561, 1993.

[72] G. Kresse and J. Furthmüller. Efficiency of *ab initio* total energy calculations for metals and semiconductors using a plane-wave basis set. *Computational Materials Science* **6**(1), pp. 15–50, 1996.

[73] G. Kresse and J. Furthmüller. Efficient iterative schemes for *ab initio* total-energy calculations using a plane-wave basis set. *Physical Review B* **54**(16), pp. 11169–11186, 1996.

[74] G. Kresse and D. Joubert. From ultrasoft pseudopotentials to the projector augmented-wave method. *Physical Review B* **59**(3), pp. 1758–1775, 1999.

[75] P. E. Blöchl. Projector augmented-wave method. *Physical Review B* **50**(24), pp. 17953–17979, 1994.

[76] G. Román-Pérez and J. M. Soler. Efficient implementation of a van der Waals density functional: application to double-wall carbon nanotubes. *Physical Review Letters* **103**(9), 096102, 2009.

[77] M. Methfessel and A. T. Paxton. High-precision sampling for Brillouin-zone integration in metals. *Physical Review B* **40**(6), pp. 3616–3621, 1989.

[78] H. J. Monkhorst and J. D. Pack. Special points for Brillouin-zone integrations. *Physical Review B* **13**(12), pp. 5188–5192, 1976.

[79] A. P. Baddorf, V. Jahns, D. M. Zehner, H. Zajonz, and D. Gibbs. Relaxation and thermal expansion of Ru(0001) between 300 and 1870 K and the influence of hydrogen. *Surface Science* **498**(1–2), pp. 74–82, 2002.